

RESEARCH ARTICLE

10.1002/2014GC005449

A family of repeating low-frequency earthquakes at the downdip edge of tremor and slip

Justin R. Sweet¹, Kenneth C. Creager¹, and Heidi Houston¹¹Department of Earth and Space Sciences, University of Washington, Seattle, Washington, USA

Key Points:

- The 9000 low-frequency earthquakes mostly locate within a circle of 300 m radius
- LFEs cluster into swarms during which amplitudes systematically increase
- Observed LFE moments yield only up to 20% of predicted slip

Supporting Information:

- Readme
- Figures S1–S10

Correspondence to:

J. R. Sweet,
jrsweet@uw.edu

Citation:

Sweet, J. R., K. C. Creager, and H. Houston (2014), A family of repeating low-frequency earthquakes at the downdip edge of tremor and slip, *Geochem. Geophys. Geosyst.*, 15, 3713–3721, doi:10.1002/2014GC005449.

Received 9 JUN 2014

Accepted 27 AUG 2014

Accepted article online 2 SEP 2014

Published online 29 SEP 2014

Abstract We analyze an isolated low-frequency earthquake (LFE) family located at the downdip edge of the main episodic tremor and slip (ETS) zone beneath western Washington State. The 9000 individual LFEs from this repeating family cluster into 198 swarms that recur roughly every week. Cumulative LFE seismic moment for each swarm correlates strongly with the time until the next swarm, suggesting that these LFE swarms are time predictable. Precise double-difference relative locations for 700 individual LFEs within this family show a distribution that is approximately 2 km long and 500 m wide, elongated parallel to the relative plate convergence direction. The distribution of locations (<300 m vertical spread) lies within a few hundred meters of two different plate interface models and has a similar dip. Peak-to-peak LFE S wave amplitudes range from 0.2 to 18 nm. Individual LFEs exhibit a trend of increasing magnitude during swarms, with smaller events at the beginning and the largest events toward the end. The largest LFEs cluster in a small area (300 m radius) coincident with maximum LFE density. We propose that the less-concentrated smaller LFEs act to unlock this patch core, allowing it to fully rupture in the largest LFEs, usually toward the end of a swarm. We interpret the patch responsible for producing these LFEs as a subducted seamount on the downgoing Juan de Fuca (JdF) plate. LFE locking efficiency (slip estimated during 5 years from summing LFE seismic moment divided by plate-rate-determined slip) is at most 20% and is highly concentrated in two ~50 m radius locations in the larger patch core. Estimated individual LFE stress drops range from 1 to 20 kPa, but could also be significantly larger.

1. Introduction

Nonvolcanic tremor—a low-frequency, long-duration seismic signal lacking distinct phase arrivals—was first identified in Japan [Obara, 2002] and has subsequently been found to correlate with deep slow slip on subduction zones in Cascadia [Rogers and Dragert, 2003] and Japan [Obara et al., 2004]. Shortly thereafter, Shelly et al. [2007] demonstrated that tremor in Japan was at least in part composed of tiny, repeating low-frequency earthquakes (LFEs). Unlike tremor, LFEs often have distinct P and S phase arrivals—a characteristic that has been exploited to accurately locate the source of LFEs and associated tremor to very near the subduction interface in Japan [Shelly et al., 2007], Cascadia, [La Rocca et al., 2009; Bostock et al., 2012], Costa Rica [Brown et al., 2009], and also on the deep extension of the San Andreas Fault near Parkfield, CA [Shelly et al., 2009]. The amplitude spectra of LFEs are deficient in high frequencies relative to similarly sized nearby earthquakes, but mirror the spectra for tremor [Kao et al., 2006; Shelly et al., 2007]. LFE focal mechanisms in Japan [Ide et al., 2007] and Cascadia [Bostock et al., 2012] are in agreement with shallow thrusting in the direction expected for plate convergence, suggesting that LFEs represent small amounts of slip on the plate interface. We create and analyze a 5 year catalog of 9000 repeats of a single LFE family to examine the behavior of slow slip on the downdip extension of the Cascadia subduction zone beneath western Washington State. This LFE family is the deepest (most downdip) and most frequently active family we have yet found. It lies on the far eastern edge of the region of PNSN tremor detections (2009–2013) [Wech, 2010] (Figure 1) and at the downdip edge of 122 LFE families located in northern Washington [Royer and Bostock, 2013]. Four of their LFE families were at similar depths, though not at the same location along strike as our LFE family. Their nearest LFE family is ~10 km south of ours, and their next nearest is ~20 km west. The frequency and regularity of our LFE family allowed us to quickly build up a large catalog of detections, making it a natural target for detailed analyses.

2. Method

We first identified this LFE through visual inspection of the data. We chose one of the highest signal-to-noise instances of this LFE and used that reference event to build up a template. A 15 s window containing

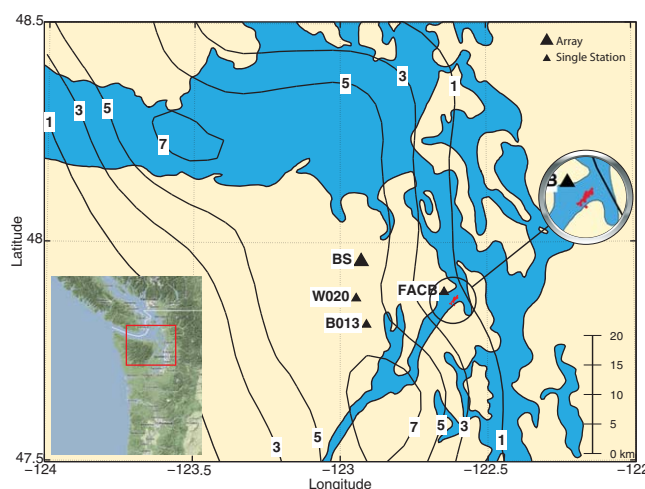


Figure 1. Map showing LFE locations (red dots), contours of 2009–2013 tremor density per square kilometer [Wech, 2010], and stations used in double-difference relocation of LFEs (triangles). There are six stations in the BS array.

the *P* and *S* waves for the reference event was autocorrelated with 12 h of data for all available channels from the 1 km aperture Big Skidder (BS) array of six 3-component stations to find matching events. This array is part of the Cascadia Arrays For Earth-Scope (CAFE) experiment. The resulting fully normalized autocorrelation functions—one for each channel—were then combined using a third-root stack to identify time windows that correlated best across all 18 channels. Templates were built by linearly stacking the 80 best correlating windows, forcing identical time offsets for each station/channel. This process was repeated three times to further improve the quality of the templates. A complete catalog was then produced using a stack of fully normalized running autocorrelations between each stacked template and its corresponding continuous 5 year long seismogram. For each day, we calculate the median of the absolute deviation (MAD) of the stacked autocorrelation function. We chose to define a detection as a time when the stacked autocorrelation function exceeded $10 \times \text{MAD}$, producing a typical threshold in which the mean correlation typically exceeded 0.2–0.3. Because the *S* minus *P* time is about 6 s, and there are often spurious detections when the *P* wave of the template aligns with the *S* wave of an LFE on the seismogram, we require the time between adjacent LFE detections to be greater than 6 s. The resulting catalog contains ~ 9600 detections. The vast majority of these are real, but a few percent appear to be erroneous, so we further filter these events as follows: (1) identify and remove events that occur within 30 s from the time of any nearby earthquakes in the Pacific Northwest Seismic Network (PNSN) catalog (~ 60 detections); (2) remove large amplitude events that occur during known periods of logging near our stations (~ 30 days in 2007); (3) remove isolated events that did not occur as part of larger LFE swarms and which were visually determined to be non-LFEs (~ 180 detections). Removing these false detections brought our final catalog size to 8942 events for the period October 2006 to September 2011. All events removed were inspected and either lacked *P* waves, *S* waves, or had an inconsistent *S* minus *P* time.

3. Temporal Distribution of LFEs: Time-Predictable Swarms

Our catalog of LFE detections is clustered into swarms of activity with $< 1\%$ of events occurring outside of swarms. We define a swarm as at least four detections such that the largest gap between detections is less than 3 h. By this metric, our 5 year catalog is organized into 198 distinct swarms with 4–268 (median of 29) LFE detections per swarm, and ~ 150 isolated, nonswarm detections, most of which are clustered into groups of 2 or 3 LFEs, which may be small, signal-poor swarms. Swarms occur roughly every 8–9 days, although interswarm times are as short as 3 h or as long as 4 weeks (supporting information Figure S1). Dividing the total number of days in our LFE catalog by the total number of swarms yields an average recurrence interval of 8 days. We define swarm duration as the time between the 10th percentile event and the 90th percentile event. Swarm durations vary from 10 min to 12 h, with a median duration of 1 h.

Interestingly, we find that cumulative seismic moment for each swarm is positively correlated with the time until the next swarm (Figure 2 and supporting information Figure S2). Seismic moment for each LFE is estimated as described in section 5 below. The definition of swarms we use in this paper is somewhat arbitrary, so we consider 40 swarm catalogs defined by the minimum number of LFEs ranging from 4 to 12 and gaps of 3–24 h between events. The mean correlation over this range of swarm definitions is 0.52 ± 0.03 . These correlations are highly significant, with *p* values ranging from 10^{-9} to 10^{-13} . These are the probabilities of achieving the observed correlations with random data. In contrast, comparing the cumulative swarm moment to the time since the last swarm for the same 40 catalogs produces correlations of 0.16 ± 0.03 , with *p* values ranging

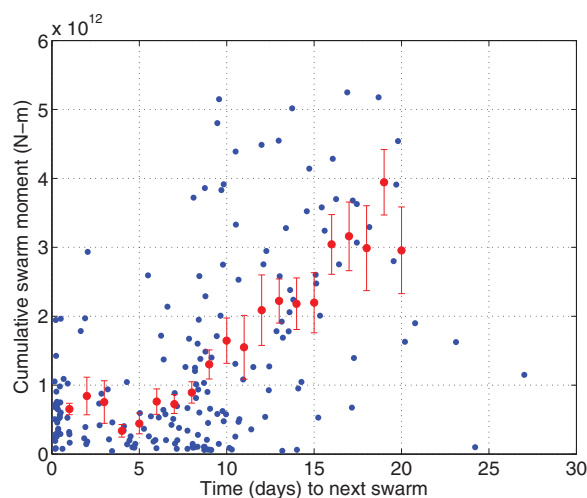


Figure 2. Cumulative swarm seismic moment versus the time (days) until the start of the next swarm for our 198-swarm catalog. The statistically significant correlation (0.51) suggests that swarms are time predictable. Increasing the minimum number of LFEs and the minimum gap between LFEs per swarm produces swarm catalogs that reduce the number of swarms clustered near the x and y axes and further improves the correlations (e.g., supporting information Figure S2a). Dots with error bars indicate mean and standard deviation of the mean for 1 day bins that contain at least four observations.

differential S and P times between stations, and S minus P times at individual stations. Using data from the BS array and from three isolated stations with noise levels small enough to record these tiny LFEs, we employed a double-difference relocation method [Waldhauser and Ellsworth, 2000] to find precise relative locations for the 700 most highly correlating events from our catalog. Our data consisted of nearly 4 million autocorrelation-obtained differential times (1.4 million for P waves, 2.6 million for S waves) measuring the time between P waves (or S waves) for all event pairs on single channels. Compared to the starting solution that had all events at the same location, the relocated events resulted in a variance reduction of 73% (supporting information Figure S3). In map view, the locations lie in a narrow patch elongated parallel to the plate convergence direction (Figure 3). The patch is approximately 2 km long and 500 m wide. Within this patch is a smaller, LFE-dense core that contains five times as many detections per square meter as the rest of the patch. The patch core is roughly circular with a radius of 300 m, and contains nearly half (46%) of the 700 relocated events. Individual LFE locations have formal errors of ~ 100 m, giving us confidence that the dimensions of our location cloud are real. The depth distribution of the locations is very small (< 300 m), suggesting that the LFEs either lie on a plane or within a narrow volume. Additionally, LFE depths are within 1 km of two different plate interface models [Preston *et al.*, 2003; McCrory *et al.*, 2012] and exhibit a similar dip angle to the east. This is consistent with nearby LFE locations from Royer and Bostock [2013]. The plate interface model of Audet *et al.* [2010] is about 5 km shallower than the LFEs.

We also calculated double-difference relocations for the best correlating events within the eight largest swarms. Among these swarms, we found five where locations migrated SW (updip), two where locations migrated NE (downdip), and two where we found no evidence for systematic migration (supporting information Figures S4–S6). Those swarms that did exhibit migration usually had speeds of ~ 1 km/h. This observation recalls previously reported tremor streaks, also seen in Cascadia, which migrate rapidly up and downdip during ETS events [Ghosh *et al.*, 2010]. While tremor streaks usually travel tens of kilometers at speeds as high as 100 km/h, our migrations are 50–100 times slower and only 1–2 km long. We postulate that a migrating pulse of slow slip is responsible for producing the LFE migrations we observe. This slow-slip pulse likely extends over an area larger than our LFE patch; however, the lack of any LFEs and/or significant tectonic tremor within 10 km of this family prevents any direct observations to measure the size of the slow-slip pulse.

from 10^{-1} to 10^{-2} . Assuming that the fault stress is steadily increasing as a result of stable plate convergence downdip, our strong correlation with time until the next swarm can be explained by a model in which there is a constant stress threshold at which a swarm of LFEs will initiate. Once a swarm has begun, it will lower the state of stress on its portion of the fault by an amount proportional to the cumulative moment of the LFEs within that swarm. Given the cumulative swarm moment and assuming a constant rate of stress loading, one can predict the amount of time until the next swarm. In other words, swarms are time predictable, not slip predictable. This behavior contrasts with previously published slip-predictable behavior of the deepest detected LFE family along the San Andreas Fault [Shelly, 2010].

4. Relative LFE Locations

To estimate the absolute location of our LFE family, we cross correlated stacked templates at different stations to measure

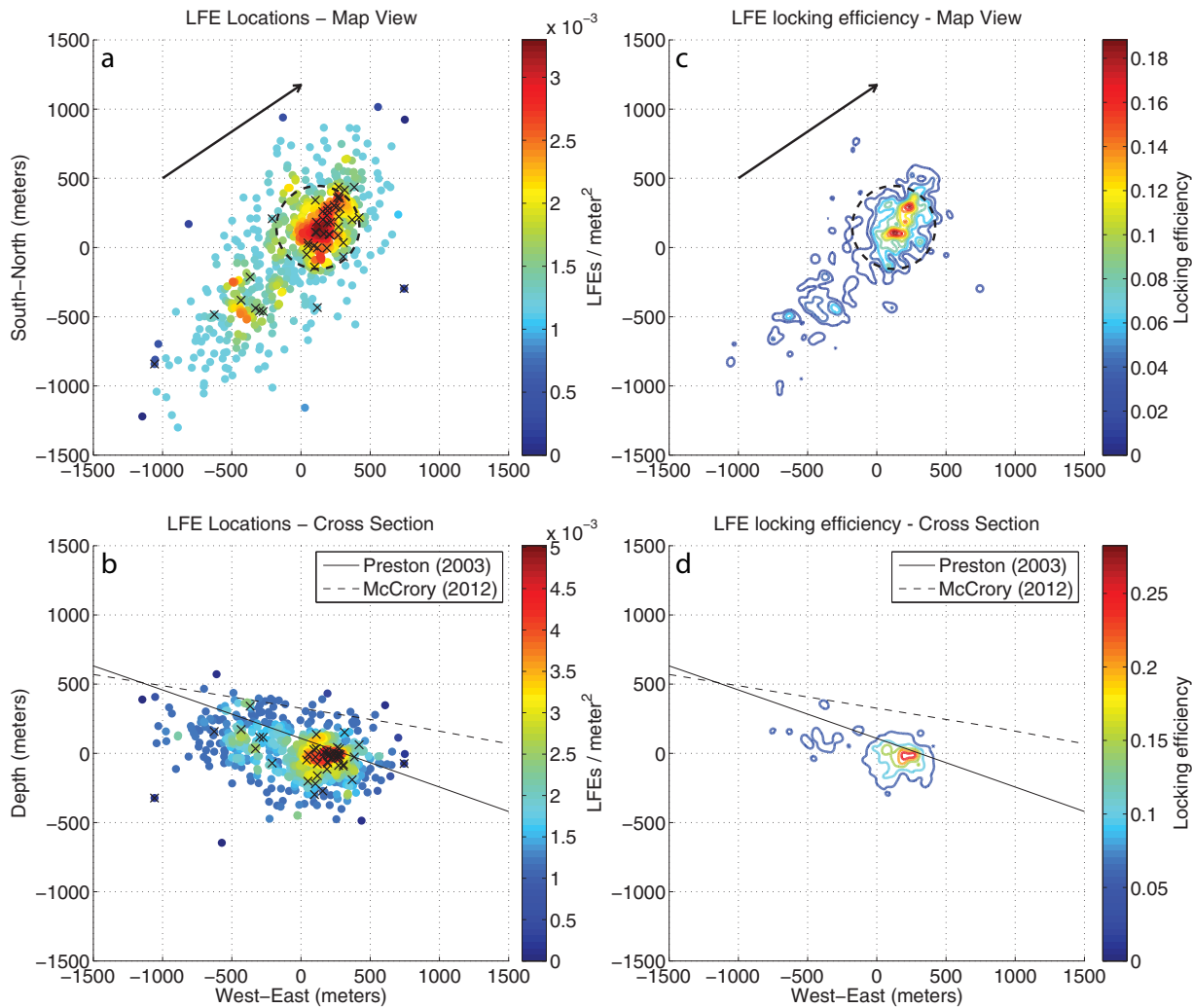


Figure 3. Locations of 700 relocated LFEs colored by density in (a) map view and (b) cross section. (c and d) LFE locking efficiency for same set of LFEs contoured at 0.05 intervals. Nearly half the LFEs lie within a 300 m radius of the patch core (dashed circle, Figures 3a and 3c). The largest 50 LFEs (black crosses, Figures 3a and 3b) cluster near the patch core. LFE distribution is elongated in the direction of plate motion (black arrow, Figures 3a and 3c) and occurs near the depths of plate interface models from *Preston et al.* [2003] (solid line, Figures 3b and 3d) and *McCrory et al.* [2012] (dashed line, Figures 3b and 3d).

5. LFE Amplitudes and Seismic Moment

To determine LFE amplitudes, we measured the peak-to-peak *S* wave amplitude on horizontal channels at six 3-component stations within the 1 km aperture BS array. All stations had instrument responses deconvolved to displacement, and were band-pass filtered from 2 to 8 Hz. The amplitude assigned to each LFE was the median peak-to-peak amplitude from the stations used for that event. To ensure accuracy, for each LFE, we only kept channels where the time of the peak amplitude matched to within 0.2 s of each other. Out of 12 total horizontal channels available, all channels were kept and used for 70% of the LFEs. We found a narrow range of LFE amplitudes that spanned from 0.2 to 18 nm. Amplitudes measured by the same method on velocity seismograms are up to 1 order of magnitude larger than LFE amplitudes reported on the San Andreas Fault (SAF) [*Shelly and Hardebeck, 2010*] despite the fact that our source-receiver distance is greater.

In order to better understand the physical characteristics of the LFE sources, we convert LFE amplitudes to seismic moment. This proved trickier than we had anticipated, primarily because high noise levels in the displacement spectra made it difficult to measure spectral values below the LFE corner frequencies. Instead, we use nearby small earthquakes to convert LFE amplitude to local magnitude (M_L) and then convert local magnitude to seismic moment.

To convert LFE amplitudes to M_L , we found eight nearby intraslab earthquakes that were also in the Pacific Northwest Seismic Network (PNSN) catalog with assigned local magnitudes. Seven of the events were located at similar depths and within 10 km of the LFEs and had M_L values between 1.2 and 1.6. The other event was a larger 4.5 magnitude earthquake that was about 17 km below the location of the LFEs. We measured median peak-to-peak S wave amplitudes for the earthquakes in the same way and at the same stations as for the LFEs. The local magnitude is based on the displacement amplitude measure on a standard Wood-Anderson seismometer, which is unusual in the sense that its response is flat to displacement at high frequencies. M_L is defined as:

$$M_L = \log_{10} A + c_1 \quad (1)$$

where A is the measured peak amplitude and c_1 is a correction for distance [Shearer, 1999]. We determine the value of c_1 for the seven small earthquakes that are all the same distance from the stations as the LFEs. For peak-to-peak amplitude A measured in meters, the earthquake-determined correction factor c_1 is 8.65 ± 0.4 .

Next, we follow the method of Shearer *et al.* [2006] who analyzed tens of thousands of small earthquakes in California, comparing catalog local magnitude values against estimates of relative seismic moment made from low-frequency spectral-amplitude measurements and found that:

$$M_L = 0.96 \log_{10} M_0 + c_2 \quad (2)$$

where M_0 is the seismic moment in Newton meters. The factor 0.96 is a robust and important result of their paper and is surprising because for moment magnitude (M_w) this factor is 0.667. The constant c_2 is determined by using the standard relationship between M_w and M_0 [Hanks and Kanamori, 1979] and assuming that M_L is equal to M_w at magnitude 3 [e.g., Shearer *et al.*, 2006]. This assumption is significant in that it determines the overall estimated moment of all the LFEs.

By combining equations (1) and (2) and rearranging terms, we arrive at an expression for converting our measured LFE amplitude A (m) to seismic moment (N m):

$$M_0 = 10^{(c_1 - c_2)1.04} A^{1.04} = 2.7 \times 10^{19} A^{1.04} \quad (3)$$

Thus, we used PNSN catalog local magnitudes to translate our observed LFE amplitudes to local magnitudes and then scaled these to seismic moment. It should be noted that due to the uncertainty in the scaling between measured LFE amplitudes and M_L , as well as between M_L and M_w , our absolute moment values are approximate and are not as well constrained as the relative moments among the events. Our calibration to M_L using seven small earthquakes has a magnitude uncertainty of ± 0.4 , and the scaling from M_L to M_w would change by 0.33 if the assumed crossover point changed by 1 unit of magnitude. Resulting LFE moments range from 2.9×10^9 N m ($M_w 0.3$) to 2.3×10^{11} N m ($M_w 1.5$). Moment magnitudes less than 1 show significant day/night variation in detection levels, suggesting that our catalog is complete above this level but incomplete below it (supporting information Figure S7).

The number of LFEs bigger than a given amplitude is better explained by an exponential distribution than by a power law distribution (Figure 4). Two previous studies of tremor and LFE amplitudes have also reported exponential amplitude distributions [Watanabe *et al.*, 2007; Shelly and Hardebeck, 2010]. Fitting a line through the power law distribution for the largest 1000 LFEs would produce a b -value (slope) of about 4, meaning that there are many more small events for a given number of big events than seen for regular earthquakes, which have b -values near 1. However, the slope varies continuously at smaller amplitudes suggesting this is not the appropriate distribution. The exponential distribution can be described as:

$$N = c_3 10^{-A/A_0} \quad (4)$$

where N is the number of LFEs with amplitude bigger than A , $A_0 \sim 4.5$ nm, and c_3 , the total number of LFEs, is about 10^4 . The average amplitude in this distribution is $\log_{10} e \times A_0 = 2$ nm. The number of events falls off by a factor of 10 for every increase in amplitude of A_0 . According to our calibration of equation (3), this increase corresponds to $M_w 1.1$, or $M_0 = 5.6 \times 10^{10}$ N m.

6. Discussion

Major episodic tremor and slip (ETS) events occur regularly in this part of Cascadia [Rogers and Dragert, 2003; Wech *et al.*, 2009], and appear to trigger activity at our LFE family, although very few tremors are

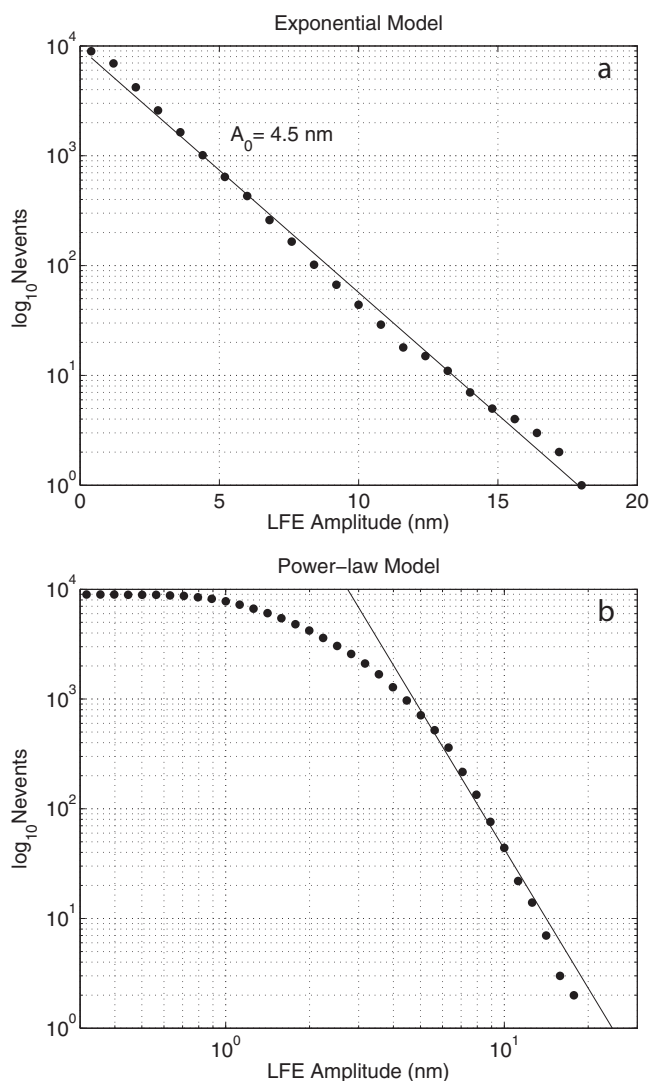


Figure 4. (a) Log linear and (b) log-log plots of number of LFEs above a given amplitude. An exponential distribution (Figure 4a) fits the observations best with characteristic amplitude of $A_0 = 4.5$ nm where $N = N_0 \times 10^{-A/A_0}$. The power law model (Figure 4b) is most consistent with a very large b value of 4.2 (black line).

in addition, the highest density of locations appears to be located on the downdip (northeastern) end of the distribution, which strongly suggests that the feature responsible for creating these LFEs resides on the downgoing Juan de Fuca (JdF) plate. In this view, the locations updip of the high-density spot can be seen as a wake of LFEs following behind the primary location of LFE generation. One possible explanation for this arrangement is the presence of a seamount, or other locally unique geologic formation on the JdF plate that is able to radiate seismically in LFEs when slipping while the adjacent areas around it are not. The fact that the distribution of LFE locations is also very thin vertically, and dips toward the east at depths coincident with several plate models, is consistent with these LFEs locating on the plate interface. The vertical spread is ~ 300 m, which could indicate the thickness of the region responsible for slow slip, but given uncertainties in relative LFE locations, the slow slip could also be confined to a much thinner fault. At any rate it is not likely to be broader than 300 m.

The finding that nearly all the LFEs occur as part of swarms, rather than isolated events, suggests that the LFEs are being externally driven, likely by small, frequent pulses of slow slip. This idea is further supported by the observed migration trends in the double-difference locations for this LFE family, which often show systematic progression updip or downdip (supporting information Figures S4–S6). The frequency of swarms

observed this far downdip during ETS. During each of the five ETS events between 2007 and 2011 in northern Washington, we detect LFE activity within 1–3 days following vigorous updip tremor activity. In four of the five cases, LFE swarms occurred. However, since swarms recur every 8 days or so, it is difficult to be definitive. Additionally, the LFE swarms observed during ETS are not systematically bigger or different than the other 50 swarms that occur over the course of each ETS cycle. We interpret the activity of this family as primarily a result of smaller but more frequent episodes of slow slip at and around the location of this LFE [e.g., *Wech and Creager, 2011*]. These small, frequent slips are likely driven by continuous slow slip just downdip of this LFE at the junction between the assumed constantly creeping zone and the tremor/LFE zone. Interestingly, we find no other detectable LFEs within 10 km of this LFE family. The isolation of this LFE family is unique, and allows us to examine detailed LFE behavior without contamination from other nearby families, as occurs in the more LFE-dense ETS zone updip.

The northeast-southwest trend of the LFE hypocenters suggests that the LFE locations are influenced by the plate convergence direction. In

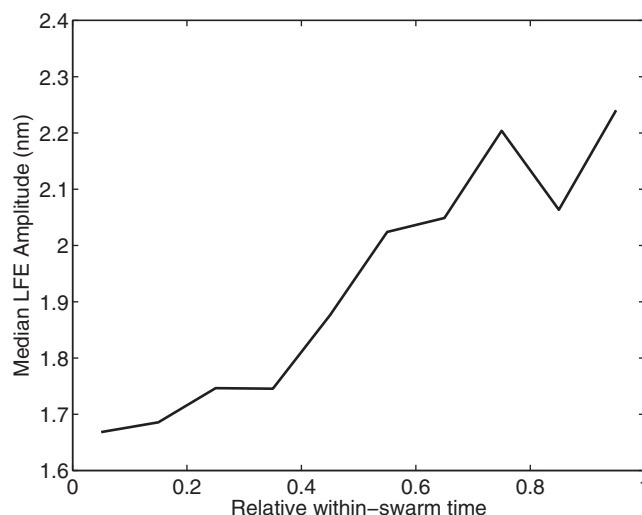


Figure 5. Individual LFEs are binned by the relative within-swarm time of their occurrence showing the median displacement amplitude. The median LFE amplitude increases systematically from the beginning to the end of a swarm—suggesting smaller events may first be needed to unlock the patch core for failure in larger events toward the end of the swarm.

patch core. A plot of the 50 largest LFEs from the 700 relocated events supports this idea by showing that most of these large LFEs are located on or near the patch core (Figures 3a and 3b). In contrast, a plot of the 50 smallest LFEs from this same set shows that they are scattered throughout the larger LFE patch (supporting information Figure S9). It should be noted that the location uncertainties for the smallest 50 LFEs are not significantly larger than those for the 50 largest LFEs. The largest LFE we detect during our 5 year data set is about M_w 1.5, which suggests that the patch dimensions do not permit larger events to occur at this location. *Rubin and Armbruster [2013]* found a similar pattern of increasing amplitudes during LFE swarms beneath southern Vancouver Island, though the LFEs they analyzed were farther updip than ours.

We use two approaches to estimate the size of the patch responsible for generating LFEs. The first approach relies on the distribution of the double-difference event locations. This distribution shows that a small area (radius \sim 300 m) contains the highest density of LFE locations. This same area also contains nearly all of the largest individual LFEs, as well as half the total moment of the entire LFE family. For these reasons, we use 300 m as one estimate of the size of the LFE patch. Our second approach relies on our estimate of the total LFE moment, as well as the plate convergence rate to derive the expected patch size. For this approach, we assume that at the location of the LFEs, the plate interface is not accumulating any stress over the 5 year period of our catalog. This implies that the amount of slip at the location of the LFEs should be equal to the slip predicted by the plate convergence rate over the same period. This is supported by the observation that the LFE moment rate does not change during our 5 year observation period. The total moment of all the LFEs in our 5 year catalog is 2.6×10^{14} N m (M_w 3.6), which is almost certainly an underestimate of the true moment release for two primary reasons. First, our catalog only keeps events separated by more than 6 s, which would fail to include even large amplitude LFEs that often occur in rapid succession. Second, based on the differing rates of detection seen for events smaller than M_w 1 during the day versus during the night, our catalog is missing some of these smaller events during noisy periods. Despite these limitations, we make use of our 5 year total moment, along with the predicted slip over the same period provided by the plate convergence rate (\sim 40 mm/yr) [*McCaffrey et al., 2007*] to estimate the average patch size responsible for the LFEs we observe. Seismic moment is defined as:

$$M_0 = \mu DA \quad (5)$$

where μ is the shear modulus, D is the amount of slip, and A is the area that slipped. We use $\mu = 3 \times 10^{10}$ N/m², which splits the difference between that expected for typical subducted oceanic crust at the

indicates that small slow-slip events at this location occur 50 times more often than the larger ETS events seen in this part of Cascadia [*Rogers and Dragert, 2003*]. If the LFEs were occurring independently, rather than being externally driven, one would expect them to occur with a more random distribution in time.

We find that the median amplitude of individual LFEs increases during a swarm by about 30% (Figure 5 and supporting information Figure S8). This suggests that in order for all or most of the patch to rupture in a single event (and thus produce a large LFE) the patch might first need to be “unlocked” by smaller ruptures from smaller LFEs prior to the full rupture. The increase in amplitude may also result from stronger coupling in the

appropriate depths (4×10^{10}) and values consistent with a highly anomalous upper oceanic crust with V_p/V_s ratios of order 2.4 [Audet *et al.*, 2009]. If the plate interface is divided into regions that only slip seismically—producing LFEs—and regions that slip totally aseismically, then the LFE generating area, determined from (5) using cumulative seismic moment and total plate-rate slip, is limited to a circle of radius 100 m. Alternatively, the LFE generating patch could sometimes slip seismically and sometimes aseismically.

In order to better understand which parts of the patch are most efficient at radiating LFEs, we estimate the LFE locking efficiency. Similar to seismic efficiency, we define the LFE locking efficiency as the proportion of the total slip that is accommodated by detected LFEs. We sum the individual moments of the 700 relocated LFEs using a Gaussian smoothing scheme that distributes the moment of each LFE over a Gaussian distribution with a half width of 25 m. This produces a map of total moment per square meter. Using equation (5) and dividing by μ delivers a map of total slip during 5 years. Assuming the actual slip on the plate interface is equal to the plate rate over the time period of our catalog, we divide our total slip by the amount predicted by plate rate to obtain LFE locking efficiency. The highest LFE locking efficiency occurs in two small (~ 50 m radius) areas and reaches only about 20% (Figures 3c and 3d). These small high-efficiency areas both fall within a larger area of elevated locking efficiency that is bounded by our 300 m radius patch core. Due to uncertainties, it is possible that most of the slip expressed as observed LFEs occurs within these two small high-efficiency areas. As mentioned previously, it is likely that the total moment we observe is less than the true moment. This could explain why the LFE locking efficiency never approaches 100%. It is likely, however, that some or most of the moment is expressed aseismically—even within our patch core.

Finally, we make use of estimates of patch size and moment to calculate the stress drop associated with a single LFE. Using the exponential distribution seen in our amplitude catalog, we select an LFE of characteristic size ($M_w 1.1$). The stress drops for a circular fault with moment magnitude 1.1 and radii of 100 and 300 m are 20 and 1 kPa, respectively [Brune, 1970] (supporting information Figure S10). These values are several orders of magnitude less than the stress drops typical for similarly sized ordinary earthquakes. If, on the other hand, we assume each LFE in a swarm ruptures only a portion of the larger patch, then the fault radius for an individual LFE could be $\ll 100$ m, yielding stress drops on the order of 10^5 or 10^6 Pa, which would be similar in size to those seen in ordinary earthquakes. It should be noted that if LFEs do have stress drops close to those of ordinary earthquakes that would not imply that LFEs and ordinary earthquakes are in other ways similar. A small stress drop makes sense given the fluid-rich, high pore pressure environment thought to exist near the plate interface in regions with detectable tremor and LFEs [Shelly *et al.*, 2006]. In fact, tidal stresses of order 1 kPa as well as stress from surface waves of large teleseismic earthquakes have been observed to strongly modulate tremor in Cascadia and elsewhere [Rubinstein *et al.*, 2007, 2008; Gomberg *et al.*, 2008].

7. Conclusion

In summary, the isolated LFE family we examined revealed a number of interesting characteristics. LFEs in this family are clustered into swarms occurring on average every week. Cumulative LFE seismic moment for each swarm correlates strongly with the time until the next swarm, suggesting that these LFE swarms are time predictable. Double-difference locations for 700 members of this family show a pattern of locations elongated parallel to the plate convergence direction. These locations dip eastward and occupy a narrow plane < 300 m thick that lies very near the location of two different plate interface models. Peak-to-peak LFE amplitudes range from 0.2 to 18 nm and correspond with moment magnitudes of 0.3–1.5. LFE amplitudes are observed to increase during swarms, with the largest events usually occurring at the end of swarms. Nearly all of the largest events locate within a 300 m radius patch core coincident with the region of highest LFE location density. We propose a model where smaller LFEs in the early part of a swarm may serve to unlock the patch core and allow it to fail at the end of the swarm in the form of a high-amplitude LFE. LFE locking efficiency indicates that a maximum of 20% of plate-rate slip is accommodated by LFEs, and only in two small patches (~ 50 m radius) within the larger patch core. Depending on assumptions, we estimate stress drops of only a few kilopascals or as high as several megapascals during individual LFEs at this location.

Acknowledgments

This work was supported by the CAFE and Array of Arrays NSF-EarthScope grants 0545441 and 0844392. Data used for this research are available at the IRIS Data Management Center. Map created using the M_map software written by Richard Pawlowicz.

References

- Audet, P., M. G. Bostock, N. I. Christensen, and S. M. Peacock (2009), Seismic evidence for overpressured subducted oceanic crust and megathrust fault sealing, *Nature*, *457*, 76–78, doi:10.1038/nature07650.
- Audet, P., M. G. Bostock, D. C. Boyarko, M. R. Brudzinski, and R. M. Allen (2010), Slab morphology in the Cascadia fore arc and its relation to episodic tremor and slip, *J. Geophys. Res.*, *115*, B00A16, doi:10.1029/2008JB006053.
- Bostock, M. G., A. A. Royer, E. H. Hearn, and S. M. Peacock (2012), Low frequency earthquakes below southern Vancouver Island, *Geochem. Geophys. Geosyst.*, *13*, Q11007, doi:10.1029/2012GC004391.
- Brown, J. R., G. C. Beroza, S. Ide, K. Ohta, D. R. Shelly, S. Y. Schwartz, W. Rabbel, M. Thorwart, and H. Kao (2009), Deep low frequency earthquakes in tremor localize to the plate interface in multiple subduction zones, *Geophys. Res. Lett.*, *36*, L19306, doi:10.1029/2009GL040027.
- Brune, J. N. (1970), Tectonic stress and the spectra of seismic shear waves from earthquakes, *J. Geophys. Res.*, *75*, 4997–5009, doi:10.1029/JB075i026p04997.
- Ghosh, A., J. E. Vidale, J. R. Sweet, K. C. Creager, A. G. Wech, H. Houston, and E. Brodsky (2010), Rapid, continuous streaking of tremor in Cascadia, *Geochem. Geophys. Geosyst.*, *11*, Q12010, doi:10.1029/2010GC003305.
- Gomberg, J., J. L. Rubinstein, Z. Peng, K. C. Creager, J. E. Vidale, and P. Bodin (2008), Widespread triggering of non-volcanic tremor in California, *Science*, *319*, 173, doi:10.1126/science.1149164.
- Hanks, T. C., and H. Kanamori (1979), A moment magnitude scale, *J. Geophys. Res.*, *84*, 2348–2350, doi:10.1029/JB084iB05p02348.
- Ide, S., D. R. Shelly, and G. C. Beroza (2007), Mechanism of deep low frequency earthquakes: Further evidence that deep non-volcanic tremor is generated by shear slip on the plate interface, *Geophys. Res. Lett.*, *34*, L03308, doi:10.1029/2006GL028890.
- Kao, H., S.-J. Shan, H. Dragert, G. Rogers, J. F. Cassidy, K. Wang, T. S. James, and K. Ramachandran (2006), Spatial-temporal patterns of seismic tremor in northern Cascadia, *J. Geophys. Res.*, *111*, B03309, doi:10.1029/2005JB003727.
- La Rocca, M., K. C. Creager, D. Galluzzo, S. Malone, J. E. Vidale, J. R. Sweet, and A. G. Wech (2009), Cascadia tremor located near plate interface constrained by S minus P wave times, *Science*, *323*, 620–623, doi:10.1126/science.1167112.
- McCaffrey, R., A. I. Qamar, R. W. King, R. Wells, G. Khazaradze, C. A. Williams, C. W. Stevens, J. J. Vollick, and P. C. Zwick (2007), Fault locking, block rotation and crustal deformation in the Pacific Northwest, *Geophys. J. Int.*, *169*, 1315–1340, doi:10.1111/j.1365-246X.2007.03371.x.
- McCrory, P. A., J. L. Blair, F. Waldhauser, and D. Oppenheimer (2012), Juan de Fuca slab geometry and its relation to Wadati-Benioff zone seismicity, *J. Geophys. Res.*, *117*, B09306, doi:10.1029/2012JB009407.
- Obara, K. (2002), Nonvolcanic deep tremor associated with subduction in southwest Japan, *Science*, *296*, 1679–1681, doi:10.1126/science.1070378.
- Obara, K., H. Hirose, F. Yamamizu, and K. Kasahara (2004), Episodic slow slip events accompanied by non-volcanic tremors in southwest Japan subduction zone, *Geophys. Res. Lett.*, *31*, L23602, doi:10.1029/2004GL020848.
- Preston, L. A., K. C. Creager, R. S. Crosson, T. M. Brocher, and A. M. Trehu (2003), Intraslab earthquakes: Dehydration of the Cascadia slab, *Science*, *302*, 1197–1200, doi:10.1126/science.1090751.
- Rogers, G., and H. Dragert (2003), Episodic tremor and slip on the Cascadia subduction zone: The chatter of silent slip, *Science*, *300*, 1942–1943, doi:10.1126/science.1084783.
- Royer, A. A., and M. G. Bostock (2013), A comparative study of low frequency earthquake templates in northern Cascadia, *Earth and Planet. Sci. Lett.*, *402*, 247–256, doi:10.1016/j.epsl.2013.08.040.
- Rubin, A. M., and J. G. Armbruster (2013), Imaging slow slip fronts in Cascadia with high precision cross-station tremor locations, *Geochem. Geophys. Geosyst.*, *14*, 5371–5392, doi:10.1002/2013GC005031.
- Rubinstein, J. L., J. E. Vidale, J. Gomberg, P. Bodin, K. C. Creager, and S. D. Malone (2007), Non-volcanic tremor driven by large transient shear stresses, *Nature*, *448*, 579–582.
- Rubinstein, J. L., M. La Rocca, J. E. Vidale, K. C. Creager, and A. G. Wech (2008), Tidal modulation of non-volcanic tremor, *Science*, *319*, 186, doi:10.1126/science.1150558.
- Shearer, P. M. (1999), *Introduction to Seismology*, pp. 182–191, Cambridge Univ. Press, New York.
- Shearer, P. M., G. A. Prieto, and E. Hauksson (2006), Comprehensive analysis of earthquake source spectra in southern California, *J. Geophys. Res.*, *111*, B06303, doi:10.1029/2005JB003979.
- Shelly, D. R. (2010), Periodic, chaotic, and doubled earthquake recurrence intervals on the deep San Andreas Fault, *Science*, *328*, 1385–1388, doi:10.1126/science.1189741.
- Shelly, D. R., and J. L. Hardebeck (2010), Precise tremor source locations and amplitude variations along the lower-crustal central San Andreas Fault, *Geophys. Res. Lett.*, *37*, L14301, doi:10.1029/2010GL043672.
- Shelly, D. R., G. C. Beroza, S. Ide, and S. Nakamura (2006), Low-frequency earthquakes in Shikoku, Japan and their relationship to episodic tremor and slip, *Nature*, *442*, 188–191, doi:10.1038/nature04931.
- Shelly, D. R., G. C. Beroza, and S. Ide (2007), Non-volcanic tremor and low frequency earthquake swarms, *Nature*, *446*, 305–307, doi:10.1038/nature05666.
- Shelly, D. R., W. L. Ellsworth, T. Ryberg, C. Haberland, G. S. Fuis, J. Murphy, R. M. Nadeau, and R. Bürgmann (2009), Precise location of San Andreas Fault tremors near Cholame, California using seismometer clusters: Slip on the deep extension of the fault?, *Geophys. Res. Lett.*, *36*, L01303, doi:10.1029/2008GL036367.
- Waldhauser, F., and W. L. Ellsworth (2000), A double-difference earthquake location algorithm; method and application to the northern Hayward Fault, California, *Bull. Seismol. Soc. Am.*, *90*(6), 1353–1368.
- Watanabe, T., Y. Hiramatsu, and K. Obara (2007), Scaling relationship between the duration and the amplitude of non-volcanic deep low-frequency tremors, *Geophys. Res. Lett.*, *34*, L07305, doi:10.1029/2007GL029391.
- Wech, A. G. (2010), Interactive tremor monitoring, *Seismol. Res. Lett.*, *81*(4), 664–669.
- Wech, A. G., and K. C. Creager (2011), A continuum of stress, strength and slip in the Cascadia subduction zone, *Nat. GeoSci.*, *4*, 624–628, doi:10.1038/ngeo1215.
- Wech, A. G., K. C. Creager, and T. I. Melbourne (2009), Seismic and geodetic constraints on Cascadia slow slip, *J. Geophys. Res.*, *114*, B10316, doi:10.1029/2008JB006090.